A possible use of melatonin in the dental field: protein adsorption and *in vitro* cell response on coated titanium

Andreia Cerqueira[1], Francisco Romero-Gavilán[1*], Nuno Araújo-Gomes[2], Iñaki García-Arnáez[3], Cristina Martinez-Ramos[4], Seda Ozturan[5], Mikel Azkargorta[6], Félix Elortza[6], Mariló Gurruchaga[3], Julio Suay[1], Isabel Goñi[3]

[1]Department of Industrial Systems Engineering and Design, Universitat Jaume I, Av. Vicent Sos Baynat s/n, 12071 Castellón de la Plana, Spain

[2]Department of Developmental Bioengineering, University of Twente, Faculty of Science and Technology, 7522LW, Enschede, The Netherlands

[3]Facultad de Ciencias Químicas, Universidad del País Vasco, P. M. de Lardizábal, 3, 20018 San Sebastián, Spain

[4]Center for Biomaterials and Tissue Engineering, Universitat Politècnica de Valencia, Camino de Vera, s/n 46022 Valencia, Spain

[5]Department of Periodontology, Faculty of Dentristy, Istambul Medeniyet University, Istanbul, Turkey

[6]Proteomics Platform, CIC bioGUNE, CIBERehd, ProteoRed-ISCIII, Bizkaia Science and Technology Park, 48160 Derio, Spain

*Corresponding author: Francisco Romero-Gavilán

Departamento de Ingeniería de Sistemas Industriales y Diseño

Campus del Ríu Sec

Avda. Vicent Sos Baynat s/n

12071 – Castelló de la Plana (España)

E-mail: gavilan@uji.es

Abstract

Melatonin (MLT) is widely known for regulating the circadian cycles and has been studied for its role in bone regeneration and inflammation. Its application as a coating for dental implants can condition the local microenvironment, affecting protein deposition on its surface and the cellular and tissue response. Using sol-gel coatings as a release vehicle for MLT, the aim of this work was to assess the potential of this molecule in improving the osseointegration and inflammatory responses of a titanium substrate. The materials obtained were physicochemically characterized (scanning electron microscopy, contact angle, roughness, Fourier-transform infrared spectroscopy, nuclear magnetic resonance, Si release, MLT liberation, and degradation) and studied *in vitro* with MC3T3-E1 osteoblastic cells and RAW264.7 macrophage cells. Although MLT application led to an increased gene expression of RUNX2 and BMP2 in 10MTL, it did not improve ALP activity. On the other hand, MLT-enriched sol-gel materials presented potential effects in the adsorption of proteins related to inflammation, coagulation and angiogenesis pathways depending on the dosage used. Using LC-MS/MS, protein adsorption patterns were studied after incubation with human serum. Proteins related to the complement systems (CO7, IC1, CO5, CO8A, and CO9) were less adsorbed in materials with MLT; on the other hand, proteins with functions in the coagulation and angiogenesis pathways, such as A2GL and PLMN, showed a significant adsorption pattern.

Keywords

Osseointegration, hybrid sol-gel, inflammation, proteomics, coating, *N*-acetyl-5-metoxy-tryptamine

1. Introduction

Dental implantations have become a standard procedure in oral rehabilitation, representing a reliable treatment with many advantages. However, implant failure still occurs, particularly in patients with poor osseointegration capability (*e.g.* patients with osteoporosis), prompting the need for bioactive surfaces that accelerate this process [1].

Titanium (Ti) and its alloys are commonly used in dental implants due to their high degree of biocompatibility. However, these materials have the limitation of being relatively bioinert and various methodologies are being studied to confer them bioactive properties. The sol-gel technique allows the synthesis of coatings to metal surfaces with a variety of functions, being an attractive method due to the use of mild reaction conditions, easily available precursors, and their potential as controlled release vehicles for ions and biomolecules [2]. Using modified alkoxysilanes as precursors, Martínez-Ibáñez et al. [3] obtained a sol-gel material by the mixture of methyltrimetoxisilane (MTMOS) and tetraethyl orthosilicate (TEOS), in a proportion of 70% MTMOS to 30% TEOS, presenting promising cellular *in vitro* behavior, with the improvement of the osseointegrative properties regarding the non-coated sand-blasted acid-etched titanium.

Melatonin (*N*-acetyl-5-metoxy-tryptamine; MLT), a widely known regulator of the circadian cycles produced by the pineal gland, has been described to play a major role on bone physiology through dual actions on osteoblasts and osteoclasts [4]. Previous studies [5–8] show that MLT upregulates the gene expression of RUNX2, BMP2, BMP6, and OCN, which have a pivotal role in osteoblast function and bone mineralization. On the other hand, MLT downregulates the expression of RANKL and upregulates OPG, leading to a restriction of osteoclast formation and increment of bone regeneration [9]. Additionally, MLT has been studied for its anti-inflammatory potential leading to the downregulation of TNFα, IL-1β, IL-6 [10,11], and iNOS [11,12], can either stimulate or inhibit angiogenesis [13,14], and it has an antioxidant potential [15]. Considering the effects of this molecule in bone and inflammatory responses, MLT has become a particularly attractive molecule to use in implants.

Upon implantation, blood/implant interactions lead to immediate protein adsorption onto the implant surface and consequently developing a provisional matrix on and around the biomaterial. The type, level, and surface conformation of the adsorbed proteins will determine the biological response and the ultimate implant outcome [16]. This adsorption is dependent on the surface properties of the material, such as wettability, roughness, and charge [17,18]. Thus, these parameters can ultimately have a determining role not only in the initial immune responses but also in other processes, such as coagulation, fibrinolysis, and the earlier stages of osteogenesis [19].

In this work, a new sol-gel material doped with several percentages of MLT (1%, 5%, 7.5%, and 10%) to be applied as a coating onto titanium substrates was developed. Then, we proceeded to perform its physiochemical study, *in vitro* characterization with MC3T3-E1 osteoblasts and RAW 264.7 macrophages, and protein adsorption patterns evaluation using proteomics. The main goal was to evaluate the potential of MLT when applied to titanium substrates for future dental field use.

2. Materials and methods

2.1. Sol-gel synthesis and sample preparation

The sol-gel route was used to obtain hybrid coatings with different percentages of MLT (1%, 5%, 7.5%, and 10%) using MTMOS and TEOS (Sigma–Aldrich, Merck KGaA, Darmstadt, Germany) as precursors. The maximum concentration of MLT was based on preliminary studies, where it was verified that melatonin showed solubility problems in concentrations higher than 10%. The network contained 70 and 30% (molar percentages) of these precursors, respectively. Melatonin was dissolved in 2-Propanol (Sigma-Aldrich) and mixed with the precursors in a volume ratio (alcohol:siloxane) of 1:1. The hydrolysis of alkoxysilanes was carried out by adding (at a rate of 1-drop s^{-1}) the corresponding stoichiometric amount of aqueous solution of 0.1N HCl (Sigma-Aldrich). The preparations were kept under stirring for 1 h and then 1 h at rest. Afterward, grade-4 Ti discs (12-mm diameter, 1-mm thick) with a sandblasted acid-etched treatment as described by Romero-Gavilán et al. [19] were used as a coating substrate. SAE-titanium discs were coated with a dip-coater (KSV DC; KSV NIMA, Espoo, Finland). The discs were immersed in the sol-gel solutions at a speed of 60 cm min^{-1}, left immersed for one minute, and removed at a 100 cm min^{-1}. To measure hydrolytic degradation and silicon/MLT liberations, coatings were prepared using glass-slides as a substrate. These were previously cleaned in an ultrasonic bath (Sonoplus HD 3200) for 20 min at 30 W with a nitric acid solution (25% volume), and then, with distilled water under the same conditions. In addition, free films of distinct materials were obtained by pouring the sol-gel solutions into non-stick Teflon molds in order to carry out their chemical characterization. Finally, all samples were cured for 2 h at 80°C.

2.2. Physicochemical characterization

To evaluated how surface topography was modified by MLT incorporation, scanning electron microscopy (SEM) with a Leica–Zeiss LEO equipment under vacuum (Leica, Wetzlar, Germany) was used. Before observation, the materials were treated with platinum sputtering to increase their conductivity. To measure surface roughness, an optical profilometer (interferometric and confocal) PLm2300 (Sensofar, Barcelona, Spain) was used in three discs of each material. For each disc, three measurements were done to calculate the average values of the Ra parameter. The contact angle was measured using an automatic contact angle meter OCA 20 (DataPhysics

Instruments, Filderstadt, Germany). An aliquot of 10 µL of Milli-Q water was deposited on the disc surface at a dosing rate of 27.5 µL s^{-1} at room temperature. Contact angles were determined using the SCA 20 software (DataPhysics Instruments, Filderstadt, Germany). Six discs of each material were studied after depositing two drops on each disc.

To chemically characterize all materials, Fourier Transform Infrared Spectroscopy (FTIR; Thermo Nicolet 6700) was carried out with an attenuated total reflection system (ATR). The spectra were measured in the 4000 and 400 cm^{-1} wavelength range. Solid-state silicon nuclear magnetic resonance spectroscopy (^{29}Si-NMR; Bruker 400 Avance III WB Plus) with a probe for solid samples of ICP-MS was used to evaluate the crosslinking degree of the obtained silicon networks. The pulse sequence for the analysis was the Bruker standard: 79.5 MHz frequency, the spectral width of 55 kHz, 2 ms contact time, and 5 s delay time. The spinning speed was 7.0 kHz. Hydrolytic degradation was evaluated by sample measuring weight loss before and after soaking them in 50 mL of distilled water (ddH_2O) at 37ºC during 1, 2, 4, and 8 weeks. The degradation of the coatings was registered by percentage (%) of mass lost in reference to the initial weight. Each data point is the average of three measurements performed in three different samples identically prepared.

To determine Si release, samples were incubated in 50 mL of Milli-Q water at 37ºC during 1, 2, 4, and 8 weeks. At these measuring points, aliquots of 50 µL were taken and measured using inductively coupled plasma mass spectrometry (ICP-MS, Agilent 7700). To measure MLT release, coated glass slides were submerged in 50 mL of Milli-Q water at 37ºC. At 0, 1, 3, 5, 8, 24, 48, 72, 96, 168, and 336 hours the absorbance was measured at 222 nm (wavelength characteristic of MLT [20]) with a Helios Omega UV-VIS (Thomas Scientific, New Jersey, USA). The measurements were carried out in triplicate.

2.3. In vitro assays

2.3.1. Cell culture

Mouse calvaria osteosarcoma MC3T3-E1 cells and mouse murine macrophage RAW 264.7 cells were cultured in at 37°C in a humidified (95%) CO_2 incubator in Dulbecco's Modified Eagle Medium (DMEM; Gibco, Life Technologies, Grand Island, NY, USA) supplemented with 1% penicillin/streptomycin (Biowest Inc., USA) and 10% FBS (Gibco, Life Technologies). After 24h, the MC3T3-E1 cells medium was replaced by osteogenic medium composed of DMEM, 1% of penicillin/streptomycin, 10% FBS, 1% ascorbic acid (5 mg mL^{-1}) and 0.21% β-glycerol phosphate. The culture medium was changed every other day. In each plate, wells with only cells were used as a control of culture conditions.

2.3.2. Cytotoxicity

Biomaterial cytotoxicity was assessed following the ISO 10993-5:2009 (Annex C) norm. MC3T3-E1 cells ($1x10^5$ cells cm^{-2}) were seeded on 96-well NUNC plates (Thermo Fisher Scientific, Waltham, MA, USA) for 24 h. The materials were also incubated for 24 h in 48-well NUNC plates (Thermo Fisher Scientific) in DMEM with 1% of penicillin/streptomycin and 10% FBS. Then, the cell culture medium was replaced with the medium exposed to the materials followed by an incubation of 24 h. To measure cell viability, the CellTiter 96® Proliferation Assay (MTS) (Promega, Madison, WI) was used according to manufacturer's guidelines. As a negative control, wells with only cells were used. As a positive control, cells were incubated in latex, a compound well known for being cytotoxic. The material was considered cytotoxic when presented cell viability below 70%.

2.3.3. Cell proliferation

To measure the effects of the biomaterials in cell proliferation, the alamarBlue™ cell viability reagent (Invitrogen, Thermo Fisher Scientific) was used. MC3T3-E1 cells were cultured in 24-well NUNC plates (Thermo Fisher Scientific) at a density of $3.5x10^4$ cells cm^{-2}. After culturing for 1, 3, and 7 days, cell proliferation was evaluated following the manufacturer's protocol. Additionally, an essay without cells was carried out to verify that the tested materials did not affect the alamarBlue™ cell viability reagent.

2.3.4. Alkaline phosphatase activity assay

To evaluate the effects of the materials in the mineralization capability of osteoblastic cells, the conversion of *p*-nitrophenylphosphate (*p*-NPP) to *p*-nitrophenol was used to assess the alkaline phosphatase (ALP) activity. MC3T3 cells were seeded onto the distinct surfaces in 24-well NUNC plates (Thermo Fisher Scientific) at a density of $3.5x10^4$ cells cm^{-2}. After culturing for 14 and 21 days, cells were rinsed twice with Dulbecco's phosphate-buffered saline (DPBS; Thermo Fisher Scientific), immersed in lysis buffer (0.2% Triton X-100, 10 mM Tris-HCl, pH 7.2) and incubated at 4°C for 10 minutes. Following centrifugation (7 min, 14000 rpm, 4°C), 100 µL of *p*-NPP (1mg mL^{-1}) in substrate buffer (50 mM glycine, 1 mM $MgCl_2$, pH 10.5) was added to 100 µL of the supernatant. After 2 h of incubation in the dark (37°C, 5% CO_2), the absorbance at 405 nm was measured using a microplate reader. Alkaline phosphatase activity was calculated using a *p*-nitrophenol in 0.02 mM sodium hydroxide standard curve. A Pierce BCA assay kit (Thermo Fisher Scientific) was used to calculate total protein content in the sample and to normalize ALP levels. The experiment was carried out in triplicate.

2.3.5. RNA extraction and cDNA synthesis

To evaluate the effects on the gene expression of osteogenic and inflammatory targets, MC3T3-E1 cells were seeded on the discs in 48-well NUNC plates (Thermo Fisher Scientific) at a density

of $3.5x10^4$ cells cm^{-2} for 7 and 14 days. RAW264.7 were seeded at a density of $30x10^4$ cells cm^{-2} for 1 day and $1.5x10^4$ cells cm^{-2} for 3 days. In each plate, wells without any material were used as control of culture conditions. Total RNA was extracted using TRIzol (1M guanidine thiocyanate, 1M ammonium thiocyanate, 3M sodium acetate, 5% glycerol, 38% aquaphenol). Briefly, 300 µL of TRIzol were added to the samples, and then they were incubated at room temperature for 5 min. Following centrifugation (5 min, 13000 rpm, 4°C), the supernatant was transferred, 200 µL of chloroform were added, and the samples were centrifuged (5 min, 13000 rpm, 4°C). The aqueous layer was mixed with 550 µL of isopropanol and kept at room temperature for 10 min. Samples were centrifuged (15 min, 13000 rpm, 4°C) and washed twice with 0.5 mL of 70% ethanol. The resulting pellet was dissolved in 30 µL of RNAse free water. RNA concentration, integrity, and quality were measured using NanoVue® Plus Spectrophotometer (GE Healthcare Life Sciences, Little Chalfont, UK). For cDNA synthesis, approximately 1 µg of total RNA was converted into cDNA using PrimeScript RT Reagent Kit (Perfect Real Time; TAKARA Bio Inc., Shiga, Japan) in a reaction volume of 20 µL. The reaction was conducted with the following conditions: 37°C for 15 min, 85°C for 5 secs, and a final hold at 4°C. The resulting cDNA quality and concentration were measured using a NanoVue® Plus Spectrophotometer (GE Healthcare Life Sciences), then diluted in DNAse-free water to a concentration suitable for reliable qRT-PCR analysis and stored at -20°C until further analysis. The experiment was carried out in quadruplicate.

2.3.6. Quantitative real-time PCR

Quantitative real-time PCRs (qRT-PCR) were carried out on 96-well plates (Applied Biosystems®, Thermo Fisher Scientific) with each sample represented by the gene of interest and one housekeeping gene (*glyceraldehyde phosphate dehydrogenase* (GAPDH)). Primers for each gene were designed using PRIMER3plus software tool (http://www.bioinformatics.nl/cgi-bin/primer3plus/primer3plus.cgi) from specific DNA sequences obtained from NCBI (https://www.ncbi.nlm.nih.gov/nucleotide/) and purchased to Thermo Fischer Scientific. Targets studied are shown in **Table 1**. Individual reactions contained 1 µL of cDNA, 0.2 µL of specific primers (forward and reverse at a concentration of 10 µM L^{-1}) and 5 µL of SYBR Premix Ex Taq (Tli RNase H Plus; TAKARA) in a final volume of 10 µL. Amplification efficiency was analyzed before qRT-PCR to optimize measurements. Reactions were carried out in a StepOne Plus™ Real-Time PCR System (Applied Biosystems®, Thermo Fisher Scientific) at 95°C for 30s, followed by 40 cycles of 95°C for 5s, 60°C for 34s, 95°C for 15s and 60°C for 60s. The data were obtained using the StepOne Plus™ Software 2.3 (Applied Biosystems®, Thermo Fisher Scientific). Fold changes were calculated using the $2^{-\Delta\Delta}$Ct method and the data was normalized in relation to the blank wells (without any material). Six technical replicates for each sample were measured.

Table 1: Quantitative real-time PCR primer sequence.

Gene symbol	Sequence	Accession number	Product length
	Housekeeping		
GAPDH	F:TGCCCCCATGTTTGTGATG R:TGGTGGTGCAGGATGCATT	XM_017321385	83
	MC3T3-E1		
BGLAP	F:AAGCAGGAGGGCAATAAGGT R:TGCCAGAGTTTGGCTTTAGG	NM_001032298	212
RUNX2	F: CCCAGCCACCTTTACCTACA R: TATGGAGTGCTGCTGGTCTG	NM_001271631	150
BMP2	F: CCCCAAGACACAGTTCCCTA R:GAGACCGCAGTCCGTCTAAG	NM_007553	169
	RAW264.7		
IL1BETA	F:GCCCATCCTCTGTGACTCAT R:AGGCCACAGGTATTTTGTCG	NM_008361	230
TNFALFA	F: AGCCCCCAGTCTGTATCCTT R:CTCCCTTTGCAGAACTCAGG	NM_001278601	212
EGR2	F:CAGGAGTGACGAAAGGAAGC R: ATCTCACGGTGTCCTGGTTC	NM_001373987	202

2.3.7. Cytokine quantification by ELISA

To evaluated the influence of the materials in tumor necrosis factor (TNF)-α and interleukin 4 (IL-4) production, RAW264.7 cells were seeded in 48-well NUNC plates (Thermo Fisher Scientific) a density of $30x10^4$ cells cm^{-2} for 1 day and $1.5x10^4$ cells cm^{-2} for 3 days. Then, the cell culture media was collected and frozen until further analysis. The concentration of these cytokines was determined using an ELISA (Invitrogen, Thermo Fisher Scientific) kit and according to the manufacturer's instructions.

2.3.8. Adsorbed protein layer

For obtaining the proteins adsorbed by the material surface, discs doped with MLT were incubated for 3 h (37 °C, 5% CO_2) in 24-well NUNC plates (Thermo Fisher Scientific) with 1 mL of human blood serum from male AB plasma (Sigma–Aldrich). After incubation, the serum was removed and the discs were washed five times with ddH_2O and once with 100 mM NaCl, 50 mM Tris–HCl, pH 7.0 to eliminate non-adsorbed proteins. The materials were washed once with an elution

(0.5 M triethylammonium bicarbonate buffer (TEAB), 4% of sodium dodecyl sulfate (SDS), 100 mM of dithiothreitol (DTT)) to obtain the adsorbed protein layer. The analysis was made in four independent replicates and each replicate was a pool of four discs. A Pierce BCA assay kit (Thermo Fisher Scientific) was used to calculate total protein content in the serum.

2.3.9. Proteomic analysis

Proteomic analysis was performed as described by Romero-Gavilán et al. [19] with slight modifications. Briefly, the eluted protein was digested in-solution, following the FASP protocol established by Wiśniewski et al. [21], and loaded onto a nanoACQUITY UPLC system (Waters, Milford, MA, USA) connected online to a mass spectrometer (Thermo Fisher ScientificEach material was analyzed in quadruplicate. Differential protein analysis was carried out using Progenesis software (Nonlinear Dynamics, Newcastle, UK), and the functional annotation of the proteins was performed using DAVID Go annotation program (https://david.ncifcrf.gov/) and PANTHER classification system (http://www.pantherdb.org/).

2.4. Statistical analysis

Based on the normal distribution and equal variance assumption test, the data were analyzed via a one-way analysis of variance (ANOVA) with a Newman-Keuls post hoc test. Results were expressed as mean ± standard deviation (SD). Statistical analysis was performed using GraphPad Prism 5.04 software (GraphPad Software Inc., La Jolla, CA, USA). The differences between 70M30T (control group) and 70M30T with different concentrations of MLT (experimental group) were considered statistically significant at $p \leq 0.05$ (*), $p \leq 0.01$ (**), and $p \leq 0.001$ (***).

3. Results

3.1. Physicochemical characterization

The sol-gel materials with MLT were successfully synthesized and well-adhering coatings were obtained as it can be observed in SEM micrographs (**Figure 1**). In these images, it can be observed that the sol-gel material has completely covered the Ti surface. Furthermore, the coatings seem to have smoothed the initial morphology of the SAE treatment, accumulating more sol-gel in the irregularities caused by the previous sandblasting. **Figure 1g** displays the contact angle measurements. With the addition of MLT to 70M30T, there was a significant increase in the contact angle in a dose-response manner. Regarding the roughness, with the incorporation of MLT, there was an increase of Ra when compared to 70M30T; however, there were no statistical differences between the coatings with a distinct amount of MLT (**Figure 1h**).

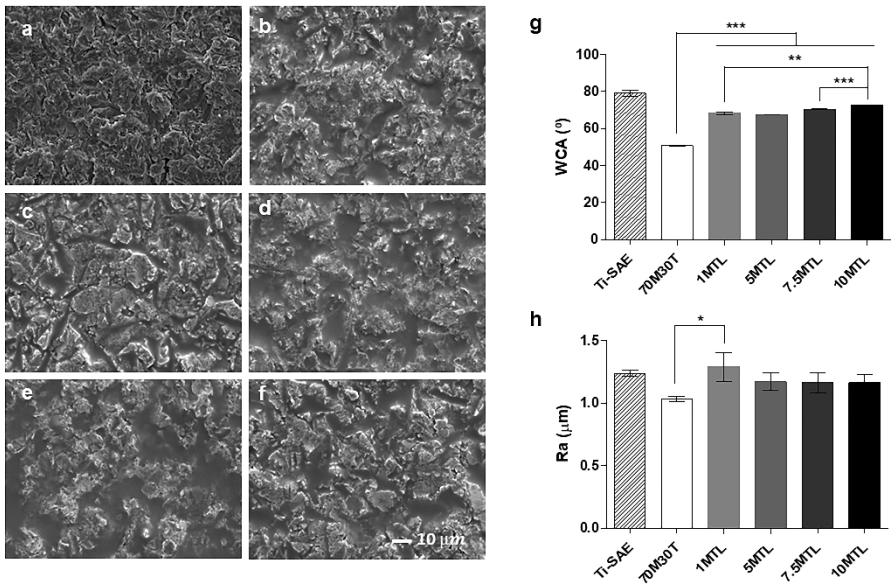

Figure 1: SEM microphotograph of Ti-SAE (a), 70M30T (b), 1MLT (c), 5MLT (d), 7.5MLT (e) and 10MLT (f) and contact angle (WCA; g) and average roughness (Ra; h). Results are shown as mean ± SD. The asterisks ($p \leq 0.05$ (*), $p \leq 0.01$ (**) and $p \leq 0.001$ (***)) indicate statistical differences in relation to 70M30T without melatonin (MLT).

3.1.1. FT-IR analysis

Sol-gel materials with different percentages of MLT were chemically characterized using FT-IR. The obtained spectra are shown in **Figure 2a**. All samples presented bands between 400 and 1200 cm^{-1}. The hydrolysis-condensation reaction was correctly carried out, as it was detected the presence of siloxane chain characteristic signals. The bands with the Si-O-Si appear proximally at 1090 cm^{-1} (asymmetric tension [22]), 770 cm^{-1} and 440cm^{-1} (symmetrical tension and vibration of deformation [23]). However, the condensation was not complete as bands at 970 cm^{-1} and 540 cm^{-1} related to the Si-OH bond of silanol groups were detected. The band related to the OH groups was observed around 3400 cm^{-1} and can be associated with the presence of water in the sol-gel structure [24]. The bands around 3000 cm^{-1} indicate the presence of C-H bonds [24], corresponding to the organic part of the MTMOS that has a methyl group (non-hydrolyzable). The band is composed of two peaks corresponding to vibrations of asymmetrical and symmetrical tension of the bond C-H. The bond associated with the Si-CH_3 group appears around 1275 cm^{-1} [25]. These methyl-associated signals show that the integrity of organic species has been maintained after processing. All identified signals are maintained and display similar intensity when the MLT is incorporated into the sol-gel. However, the materials with MLT show bands between 1500-1600 cm^{-1}, which corresponds to the CO group present in this molecule [26]. In addition, the spectra of these materials show bands at 1610 cm^{-1} and 1555 cm^{-1}, which correspond

to N-H and C-N bounds present in MLT, correspondingly [23]. The intensity of these bands is slightly more intense as the amount of melatonin increases.

Figure 2b represents ^{29}Si solid NMR spectra of 70M30T and 70M30T supplemented with MLT. These spectra show T^n signals from MTMOS and Q^n signals from TEOS. The MTMOS spectra show T^2 and T^3 signals with higher intensity of T^3. Additionally, the spectra show Q^3 and Q^4 from TEOS, with a signal more intense in Q^3. It seems that the addition of MLT to the sol-gel network did not affect the final crosslinking degree of structure.

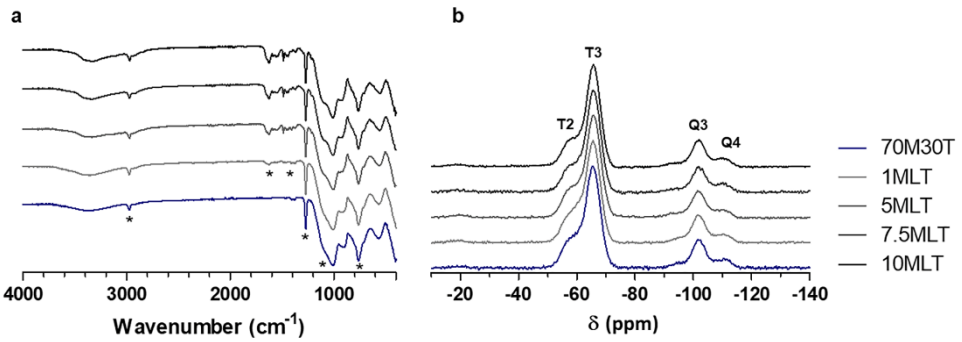

Figure 2: FT-IR spectra (a) and Si-NMR (b) of 70M30T with different concentrations of melatonin (MLT).

3.1.2. Hydrolytic degradation

Figure 3a shows the hydrolytic degradation (mass loss) of all materials for 56 days. All materials degraded and showed a significant mass loss during the first seven days. During the following days and until the end of the experiment, all materials lost weight in a more gradually. In the case of 70M30T, the mass loss was small (up to 16%), while the materials with MLT showed a higher weight loss. In these coatings, the degradation increased as the percentage of MLT in the network increased. Thus, the 10MLT showed the highest degradation in all materials studied.

3.1.3. Silicon and melatonin liberation

Figure 3b shows the liberation of silicon (Si released in mg L^{-1}) of all materials in the study. All materials showed a significant Si liberation during the first week. The base material 70M30T and 1MLT presented a similar liberation rate, reaching its maximum at 3 weeks. For the rest of the materials, the liberation was more gradual over the two months of the assay. Similarly, to the hydrolytic degradation, the material with a higher concentration of MLT released more Si (12.5 mg Si L^{-1} in 10MLT in two months of assay). **Figure 3c** shows MLT liberation for all materials. In similarity to the previously described parameters, MLT release showed a dose-response rate *i.e.* the material with the highest percentage (10MLT) presented the highest liberation of MLT. Considering the liberation kinetics, MLT was released faster in the first 72 h and, for this time

point onward, it had a liberation rate almost constant until the end of the assay (336 h) in all materials.

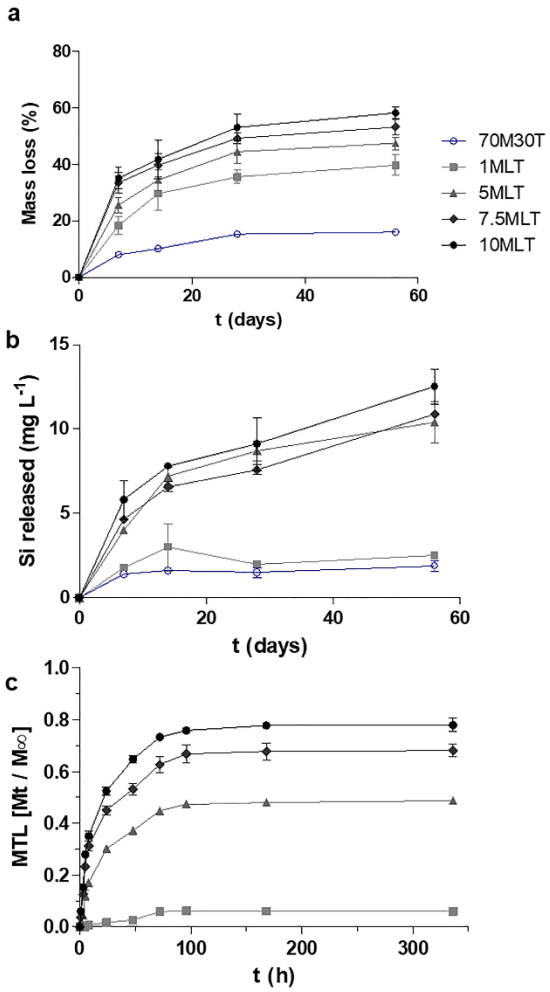

Figure 3: Hydrolytic degradation (a) of the sol-gel coating and kinetic liberation of silicon (b) and MLT (c) from the sol-gel coating through time.

3.2. *In vitro* assays

3.2.1. Cytotoxicity, cell proliferation, and ALP activity

Neither of the materials in the study was cytotoxic (data not shown). Cell proliferation and ALP activity assays did not show significant differences between the 70M30T with or without melatonin (**Figure 4**) in any measuring points.

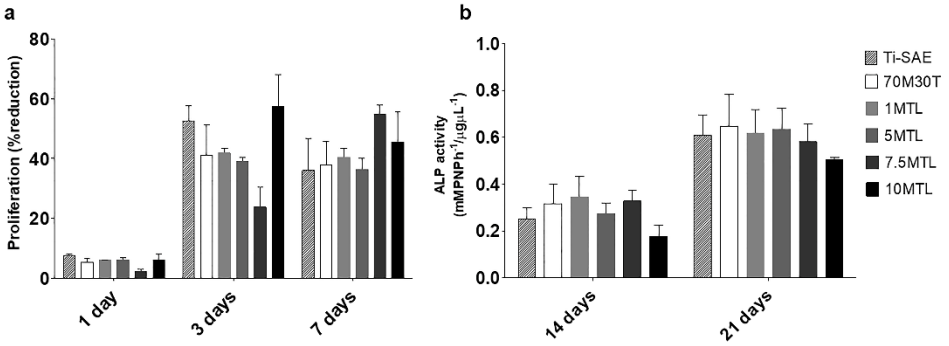

Figure 4: MC3T3-E1 *in vitro* assays: (a) cell proliferation at 1, 3, and 7 days and (b) ALP activity at 14 and 21 days. Results are shown as mean ± SD.

3.2.2. Relative gene expression

The expression of osteogenic and inflammation markers of the MC3T3-E1 and RAW264.7 cells cultured onto the distinct formulations is shown in **Figure 5**. After 14 days, all materials with MLT show a significant decrease in BGLAP expression (**Figure 5a**). On the other hand, RUNX2 and BMP2 expression showed an increase in 10MLT at 7 days. At 14 days, RUNX2 expression increased in 10MLT, while BMP2 expression decreased in all materials (**Figure 5b and c**). The expression of IL-1β and TNF-α showed no differences in any material at both time points (**Figure 5 d and e**). In the ERG2 expression, there was an increase in 7.5MLT at 1 day, while all materials showed a significant decrease at 3 days (**Figure 5f**).

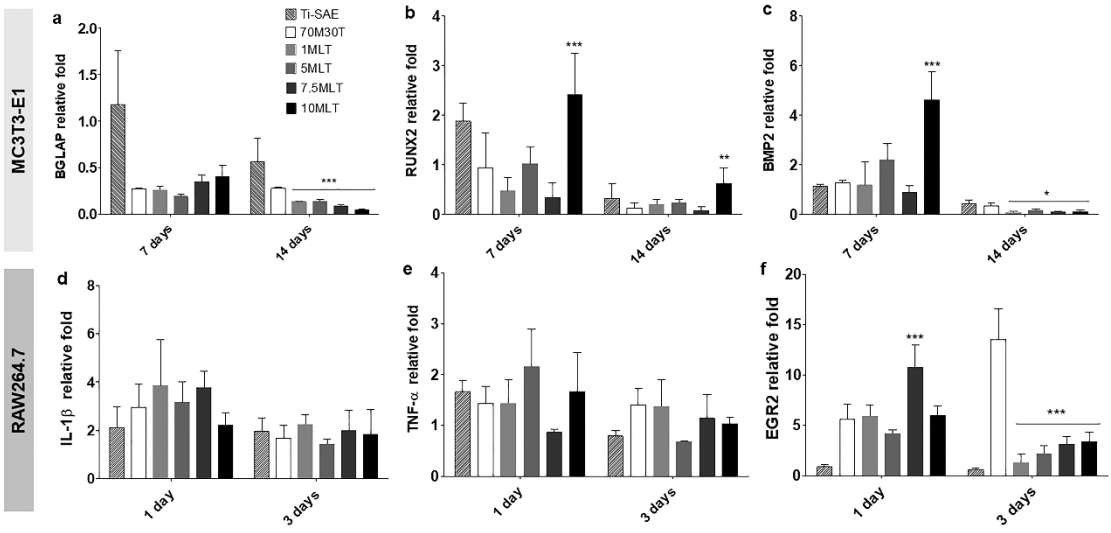

Figure 5: Relative gene expression of osteocalcin (BGLAP; a), runt-related transcription factor 2 (RUNX2; b), and bone morphogenetic protein (BMP2; c) in MC3T3 at 7 and 14 days and interleukin- 1β (IL-1β; d), tumor necrosis α (TNF-α), and early growth response protein 2 (EGR2; f) in RAW264.7 at 1 and 3 days. Results are shown as mean ± SD and were normalized to the wells without materials (bottom of cultivation

plate). The asterisks ($p \leq 0.05$ (*) and $p \leq 0.001$ (***)) indicate statistical differences in relation to 70M30T without melatonin (MLT).

3.2.3. Cytokine quantification by ELISA

To evaluate the effect of the materials with MLT on the inflammatory response, the secretion of anti (IL-4) and pro-inflammatory (TNF-α) cytokines by RAW264.7 macrophage was quantified at 1 day and 3 days. The secretion of IL-4 did not show differences at any of the times measured in any of the materials tested (**Figure 6a**). In the case of TNF-α, the profile was similar at 1 day for all materials (**Figure 6b**). After 3 days of culture, there is a general increase in the production of this cytokine; however, is significantly lower in 1% MLT when compared to the 70M30T coating.

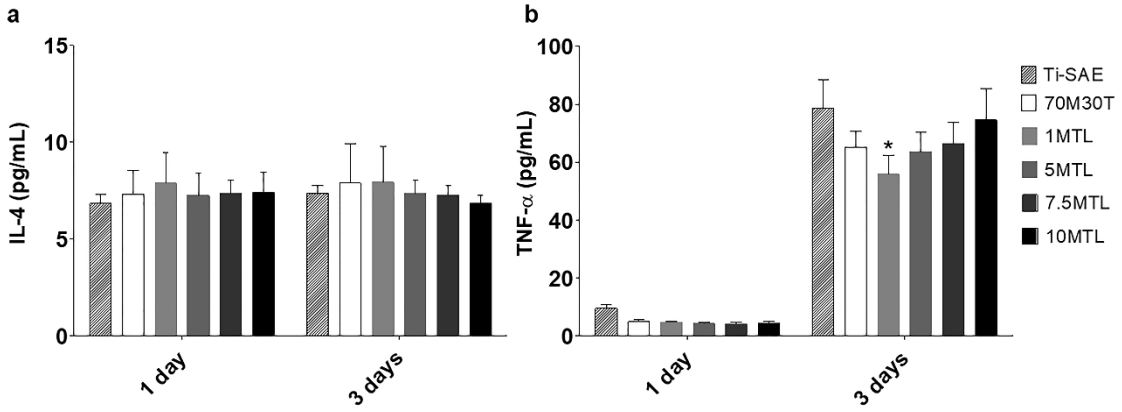

Figure 6: Cytokine quantification by ELISA in RAW264.7 at 1 and 3 days: (a) interleukin-4 (IL-4) and (b) tumor necrosis α (TNF-α). Results are shown as mean ± SD. The asterisk ($p \leq 0.05$ (*)) indicates statistical differences in relation to 70M30T without melatonin (MLT).

3.2.4. Proteomic analysis

The eluted proteins were analyzed by LC-MS/MS, followed by identification with Progenesis QI software and DAVID system. Comparing MLT-enriched and the base sol-gel material, 26 proteins were differentially absorbed in the materials with MLT (**Supplementary Table 1**). The formulation with 10MLT shows the higher amount of differently absorbed proteins, with 16 proteins being less adsorbed onto its surface and five showing more affinity. Among the proteins with decreased adsorption, five are related to the complement system (CO7, IC1, CO5, CO8A, and CO9). On the other hand, these surfaces lead to higher adsorption with CXCL7, which plays a crucial role in neutrophil recruitment. Also related to immunological responses, the surface 1MLT and 5MLT showed a higher affinity with IGHA2, while 7.5MLT differentially absorbed CO5, IC1, CO8A, and CXCL7. The glycoproteins VTCN and SEPP1 were significantly less adsorbed in the material with 10MLT, while HEMO show higher affinity with the materials with 1MLT, 5MLT, and 10MLT. VTNC is known to inhibit/regulate the complement system

activation. Depending on the concentration of MLT, the materials adsorbed fewer apolipoproteins (APOA-I, APOF, APOL1, and APOC4) and PON1. These proteins are related to the metabolism of high-density lipids. Regarding the coagulation process, HRG, HBB, PLMN, and KLKB1 were differentially adsorbed: HRG was more adsorbed in 1MLT, while KLKB1 was more adsorbed in 5MLT. In 7.5MLT and 10MLT proteins related to this process presented less affinity with these materials. Additionally, all materials except 7.5MLT showed a differential affinity with A2GL, a protein-related with the angiogenesis processes. The materials 1MLT and 5MLT adsorbed more of this protein, while 10MLT adsorbed less. ITIH2, ITIH4, and ITHI1, proteins from the inter-α-trypsin inhibitor family related to the hyaluronan metabolic process, were less adsorbed in the materials with 10MLT. ATPA, a mitochondrial membrane complex that produces ATP from ADP, was significantly more adsorbed in 1MLT. **Table 1** summarizes the most relevant proteins related to immune responses, coagulation, and angiogenesis processes found differentially absorbed onto each material surface.

PANTHER analysis was used to associate the differentially adsorbed proteins with their functions in distinct biological pathways. **Figure 7** shows pie-chart diagrams of the biological processes related to the proteins differentially adsorbed onto each surface when compared with 70M30T without MLT. ATP synthesis, blood coagulation, plasminogen activation, and B cell activation where the cascades identified and varied according to the concentration of MLT employed. In general, all materials showed less adsorbed proteins associated with blood coagulation, plasminogen activation; also, at higher concentrations of MLT (7.5 and 10), there was a general decrease of proteins associated with B cell activation pathways. Only the materials 1MLT and 5MLT showed significantly higher adsorption of proteins associated with the biological process: ATP synthesis (1MLT) and blood coagulation (5MLT).

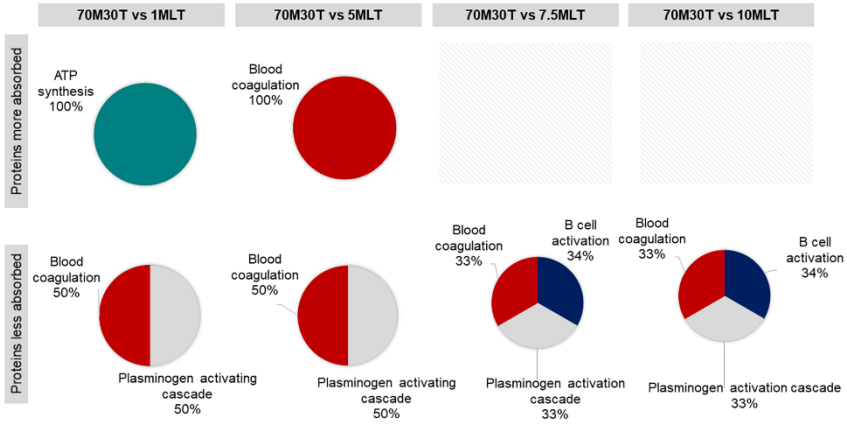

Figure 7: PANTHER diagram of the pathways associated with the proteins differentially adherent to MLT enriched coatings in comparison with 70M30T without MLT.

Table 1. Summary of the proteins of interest differentially adsorbed related to the immune, coagulation, and angiogenesis process differentially adsorbed onto each material surface when compared with 70M30T without MLT. MLT/70M30T ratios are shown between parentheses; red indicates more adsorbed, and green indicates less adsorbed.

70M30T vs 1MLT	70M30T vs 5 MLT	70M30T vs 7.5 MLT	70M30T vs 10 MLT
Immune			
IGHA2 (2.56)	IGHA2 (2.83) CXCL7 (1.65)	CO5 (0.66) CO8A (0.66) CXCL7 (2.67)	CO7 (0.46) IC1 (0.49) CO5 (0.57) VTNC (0.64) CO9 (0.66) CXCL7 (2.45)
Angiogenesis and coagulation			
HRG (1.60) A2GL (3.48)	A2GL (4.46) KLKB1 (2.91)	HBB (0.63)	HRG (0.36) A2GL (0.43) HBB (0.46) PLMN (0.51)

4. Discussion

In oral rehabilitation, dental implants have become a common procedure with many advantages. However, there is a need for bioactive surfaces that accelerate osseointegration because failure still occurs in patients somehow compromised. These surfaces can be obtained with a battery of techniques, such as sol-gel, and allow the usage of a diversity of biomolecules such as MLT. Melatonin has a wide variety of biological actions and its well-described properties have made it an attractive molecule for application in delivery systems in dentistry and regenerative medicine [27]. Considering this, the aim of the study was to develop a sol-gel coating (70M30T) supplemented with different percentages of MLT and characterize its effects in osteoblastic and immune cells, which are essential to determinate implant outcome.

The incorporation of MLT onto the 70M30T base introduced physicochemical changes in the surface properties, such as wettability. The contact angle significantly increased in relation to the base regardless of the concentration of MLT, surely by the organic character of this molecule. Regarding the material roughness, there is only a significant increase when comparing 70M30T with 1MLT. The ^{29}Si solid NMR shows that the incorporation of MLT did not affect the formation of the sol-gel network and FTIR analysis shows that it is present in the material. The hydrolytic degradation and the Si release increased in a dose-response manner with the amount of MLT incorporated in the network. This can be related to the liberation of MLT that also presented an increasing dose-response pattern depending on the amount of MLT initially added into the coating. The measured release kinetics can help to understand how melatonin is going to be

466 released *in vitro* from different materials, although the complexity of the medium employed for
467 these essays may affect this liberation.

468 In cancer cells, the inhibitory effect of this MLT on cell proliferation is well documented [28]. In
469 osteoblasts (hFOB 1.19), MLT showed an inhibitory effect on proliferation in a time-dependent
470 manner, acting in genes related to the cell division cycle [29]. Zhang et al. [20] showed that MLT
471 encapsulated in PLGA microspheres does not affect the proliferation of hMSCs at 1, 3, and 6
472 days, which is in accordance with our results. To understand how MLT affects the mineralization
473 of osteoblasts, ALP activity assay was performed. Our results show that MLT did not significantly
474 affect ALP activity at 14 and 21 days. Previous studies have shown MLT can increase ALP
475 activity in MC3T3-E1 at 14 days [30] or with 50 nM of MLT for 3 days [8]; however, these
476 findings are for when cultures are directly treated with the compound and at short times of
477 incubation (<14 days) with MLT. On the other hand, Zhang et al. [20] presented a significantly
478 higher ALP activity in MLT encapsulated microspheres at 12 days. In what concerns gene
479 expression, our results show an increase in BMP2 and RUNX2 expression in 10MTL. These
480 markers have important roles in osteoblast differentiation, and previous works [4,8,31] showed
481 that MLT can lead to their upregulation. However, further studies are needed to understand how
482 MLT affects cells in long-term exposition (>14 days) and how the incorporation in distinct release
483 vehicles affects its action.

484 The LC-MS/MS characterization of the protein layers identified 26 proteins that were
485 differentially absorbed in the materials with MLT. How and which proteins were adsorbed onto
486 each surface depended on the amount of MLT incorporated on the sol-gel network. These proteins
487 have functions associated with distinct biological pathways as shown in the PANTHER analysis.
488 Apolipoproteins APOA-I, APOF, APOL1, and APOC4 were generally less adsorbed onto the
489 surfaces with MLT. These proteins are known for their role in the metabolism of lipids, this
490 protein family might also play a role in inhibiting complement system activation [32]. APOA-I is
491 a major component of HDL that has been shown to inhibit LPS induced release of cytokines in
492 monocytes [33], revealing an anti-inflammatory potential.

493 In addition, it was found differential adsorption of complement system proteins. In the materials
494 with 7.5MLT and 10MLT, we could observe a decrease in the adsorption of complement C5
495 (CO5), complement component C8 alpha chain (CO8A), complement component (CO7) and
496 component complement (CO9). The activation of C5 initiates an assembly with late-phase
497 complement components, such as C6, C7, C8, and C9, leading to the formation of C5-C9
498 complex, a multimolecular structure that leads to the formation of the lytic complex that will be
499 responsible for the target cell lysis [34]. This is in agreement with the analysis PANTHER, which
500 shows that the proteins less adsorbed by these materials have functions associated with B cell

activation. The distinct complement pathways originate C3 and C4 fragments, which bind to complement receptors CD21 and CD35, whose co-expression is limited to B cells and leads to the enhancement of the activity of these cells [35,36]. On the other hand, vitronectin (VTNC) was less adsorbed in the materials with 10MLT. This protein has been described as an inhibitor of complement system action in bodily fluids [37]. Thus, the lower adsorption of complement proteins associated with the lower adsorption of VTNC can explain how the release of TNF-α and IL-4 cytokines by macrophage in contact with the 10MLT showed no statistical differences with respect to the base coating. Although, the anti-inflammatory potential of MLT is well described [11,38,39], its application in biomaterials can be dependent on the amount of hormone released by the material over time, and further studies are needed.

Coagulation and angiogenesis are key processes in bone regeneration. Proteomic analysis showed that MLT enriched materials differently adsorbed proteins related to both of these processes. In this sense, A2GL, a protein implicated in angiogenesis [40], was found to be more adsorbed onto the coatings 1MLT and 5MLT, but then, reduced its affinity with respect to the base material when 10% of MLT was incorporated. *In vitro*, MLT was reported to inhibit angiogenesis in cancer cells [41,42]. On the other hand, Ramírez-Fernandez et al. [14] reported that MLT promoted this process in rabbit tibiae following implantation of melatonin implants.

Regarding the coagulation process, HRG, which modulates various components in the coagulation cascade, such as heparin, increased its affinity for 1MLT. Similarly, KLKB1 was significantly more adsorbed onto the material 5MLT. This protein activates the coagulation cascade through the intrinsic pathway [43]. However, both KLKB1 and HRG reduced the affinity by the material when 10% of MLT was added.

Fibrinolysis is a highly regulated enzymatic process of clot removal tightly related to blood coagulation [44]. PLMN, a protein found less adsorbed onto 10MLT, has a role in tissue regeneration by dissolving preformed fibrin clots and extracellular matrix components allowing tissue remodeling [45]. These adsorption patterns are corroborated with PANTHER analysis, which showed a general decrease in proteins with functions related to blood coagulation and plasminogen activation.

MLT has a complex biological role and its potential effect on important pathways, such as inflammation, coagulation, and angiogenesis, in the early stages of tissue regeneration, can determine how these processes will be carried out around an implant. However, its specific mechanism of action, timings, and doses needed to produce significant cellular effects still need further studies.

5. Conclusions

In this article, we developed new coatings with MLT to be applied in titanium dental implants using a hybrid sol-gel network as a release vehicle. The addition of MLT changed the superficial parameters of the coatings, with the coatings supplemented with the hormone showing a lower hydrophilia when compared to the base material. These materials revealed to be not cytotoxic and showed an increase BMP2 and RUNX2 gene expression in 10MLT. However, osteoblastic cells did not show an improvement in the capacity of proliferation and mineralization (ALP activity) *in vitro* when exposed to the coatings. The proteomic analysis of protein adsorption onto the materials showed differences in the adsorption patterns in proteins associated with the complement pathway when MLT added and in a dose-response manner. This behavior can explain the liberation of TNF-α, which was significantly lower in the 1MLT composition. In addition, it was found differences in adsorption of proteins related to coagulation and angiogenesis, which points out a possible effect of MLT in the activation and development of these pathways.

6. Acknowledgments

This work was supported by MINECO [MAT MAT2017-86043-R; RTC-2017-6147-1], Universitat Jaume I under [UJI-B2017-37; POSDOC/2019/28], Generalitat Valenciana [GRISOLIAP/2018/091], University of the Basque Country under [UFI11/56] and Basque Government under [PRE_2017_2_0044]. CIC bioGUNE is supported by Basque Department of Industry, Tourism and Trade (Etortek and Elkartek programs), the Innovation Technology Department of the Bizkaia County; The ProteoRed-ISCIII (Grant PRB3 IPT17/0019); CIBERehd Network and Severo Ochoa Grant (SEV-2016-0644). Authors would like to thank Antonio Coso (GMI-Ilerimplant) for their inestimable contribution to this study, and Raquel Oliver, Jose Ortega (UJI) and Iraide Escobes (CIC bioGUNE) for their valuable technical assistance.

7. References

[1] R. Smeets, B. Stadlinger, F. Schwarz, B. Beck-Broichsitter, O. Jung, C. Precht, F. Kloss, A. Gröbe, M. Heiland, T. Ebker, Impact of Dental Implant Surface Modifications on Osseointegration, Biomed Res. Int. 2016 (2016) 1–16. https://doi.org/10.1155/2016/6285620.

[2] J.A. Oshiro Junior, M. Abuçafy, E. Manaia, B. Da Silva, B.G. Chiari-Andréo, L.A. Chiavacci, Drug delivery systems obtained from silica based organic-inorganic hybrids, Polymers (Basel). 8 (2016) 91. https://doi.org/10.3390/polym8040091.

[3] M. Martínez-Ibáñez, M.J. Juan-Díaz, I. Lara-Saez, A. Coso, J. Franco, M. Gurruchaga, J. Suay Antón, I. Goñi, Biological characterization of a new silicon based coating developed for dental implants, J. Mater. Sci. Mater. Med. 27 (2016). https://doi.org/10.1007/s10856-

016-5690-9.

[4] S. Maria, A. Witt-Enderby, P, Melatonin effects on bone: Potential use for the prevention and treatment for osteopenia, osteoporosis, and periodontal disease and for use in bone-grafting procedures, J. Pineal Res. 56 (2014) 115–125. https://doi.org/10.1111/jpi.12116.

[5] J.A. Roth, B.G. Kim, W.L. Lin, M.I. Cho, Melatonin promotes osteoblast differentiation and bone formation, J. Biol. Chem. 274 (1999) 22041–22047. https://doi.org/10.1074/jbc.274.31.22041.

[6] S. Sethi, N.M. Radio, M.P. Kotlarczyk, C.-T. Chen, Y.-H. Wei, R. Jockers, P.A. Witt-Enderby, Determination of the minimal melatonin exposure required to induce osteoblast differentiation from human mesenchymal stem cells and these effects on downstream signaling pathways, J. Pineal Res. 49 (2010) 222–238. https://doi.org/10.1111/j.1600-079X.2010.00784.x.

[7] L. Zhang, P. Su, C. Xu, C. Chen, A. Liang, K. Du, Y. Peng, D. Huang, Melatonin inhibits adipogenesis and enhances osteogenesis of human mesenchymal stem cells by suppressing PPARγ expression and enhancing Runx2 expression, J. Pineal Res. 49 (2010) 364–372. https://doi.org/10.1111/j.1600-079X.2010.00803.x.

[8] K.H. Park, J.W. Kang, E.M. Lee, J.S. Kim, Y.H. Rhee, M. Kim, S.J. Jeong, Y.G. Park, S. Hoon Kim, Melatonin promotes osteoblastic differentiation through the BMP/ERK/Wnt signaling pathways, J. Pineal Res. 51 (2011) 187–194. https://doi.org/10.1111/j.1600-079X.2011.00875.x.

[9] Z. Ping, Z. Wang, J. Shi, L. Wang, X. Guo, W. Zhou, X. Hu, X. Wu, Y. Liu, W. Zhang, H. Yang, Y. Xu, Y. Gu, D. Geng, Inhibitory effects of melatonin on titanium particle-induced inflammatory bone resorption and osteoclastogenesis via suppression of NF-κB signaling, Acta Biomater. 62 (2017) 362–371. https://doi.org/10.1016/j.actbio.2017.08.046.

[10] M. Kadena, Y. Kumagai, A. Vandenbon, H. Matsushima, H. Fukamachi, N. Maruta, H. Kataoka, T. Arimoto, H. Morisaki, T. Funatsu, H. Kuwata, Microarray and gene co-expression analysis reveals that melatonin attenuates immune responses and modulates actin rearrangement in macrophages, Biochem. Biophys. Res. Commun. 485 (2017) 414–420. https://doi.org/10.1016/j.bbrc.2017.02.063.

[11] Y. Xia, S. Chen, S. Zeng, Y. Zhao, C. Zhu, B. Deng, G. Zhu, Y. Yin, W. Wang, R. Hardeland, W. Ren, Melatonin in macrophage biology: Current understanding and future perspectives, J. Pineal Res. 66 (2019) 1–21. https://doi.org/10.1111/jpi.12547.

602 [12] R. Hardeland, Melatonin and inflammation—Story of a double-edged blade, J. Pineal Res.
603 65 (2018) 1–23. https://doi.org/10.1111/jpi.12525.

604 [13] Q. Ma, R.J. Reiter, Y. Chen, Role of melatonin in controlling angiogenesis under
605 physiological and pathological conditions, Angiogenesis. 23 (2019) 91–104.
606 https://doi.org/10.1007/s10456-019-09689-7.

607 [14] M.P. Ramírez-Fernández, J.L. Calvo-Guirado, J. Eduardo-Maté Sánchez de-Val, R.A.
608 Delgado-Ruiz, B. Negri, G. Pardo-Zamora, D. Peñarrocha, C. Barona, J. Manuel Granero,
609 M. Alcaraz-Baños, M.P. Ramírez-Fernández, J.L. Calvo-Guirado, B. Negri, G. Pardo-
610 Zamora, J.M. Granero, J.S. E-M de-Val, R.A. Delgado-Ruiz, D. Peñarrocha, C. Barona,
611 M. Alcaraz-Baños, H. Morales Meseguer, Melatonin promotes angiogenesis during repair
612 of bone defects: a radiological and histomorphometric study in rabbit tibiae, Clin. Oral
613 Investig. 17 (2013) 147–158. https://doi.org/10.1007/s00784-012-0684-6.

614 [15] R.J. Reiter, J.C. Mayo, D.X. Tan, R.M. Sainz, M. Alatorre-Jimenez, L. Qin, Melatonin as
615 an antioxidant: under promises but over delivers, J. Pineal Res. (2016) 253–278.
616 https://doi.org/10.1111/jpi.12360.

617 [16] N. Araújo-Gomes, F. Romero-Gavilán, I. García-Arnáez, C. Martínez-Ramos, A.M.
618 Sánchez-Pérez, M. Azkargorta, F. Elortza, J.J. Martín de Llano, M. Gurruchaga, I. Goñi,
619 J. Suay, Osseointegration mechanisms: a proteomic approach, JBIC J. Biol. Inorg. Chem.
620 23 (2018) 459–470. https://doi.org/10.1007/s00775-018-1553-9.

621 [17] Z. Sheikh, P.J. Brooks, O. Barzilay, N. Fine, M. Glogauer, Macrophages, foreign body
622 giant cells and their response to implantable biomaterials, Materials (Basel). 8 (2015)
623 5671–5701. https://doi.org/10.3390/ma8095269.

624 [18] F. Romero-Gavilán, N. Araújo-Gomes, A. Cerqueira, I. García-Arnáez, C. Martínez-
625 Ramos, M. Azkargorta, I. Iloro, M. Gurruchaga, J. Suay, I. Goñi, Proteomic analysis of
626 calcium ‐ enriched sol – gel biomaterials, JBIC J. Biol. Inorg. Chem. 24 (2019) 563–574.
627 https://doi.org/10.1007/s00775-019-01662-5.

628 [19] F. Romero-Gavilan, A.M. Sánchez-Pérez, N. Araújo-Gomes, M. Azkargorta, I. Iloro, F.
629 Elortza, M. Gurruchaga, I. Goñi, J. Suay, Proteomic analysis of silica hybrid sol-gel
630 coatings: a potential tool for predicting the biocompatibility of implants *in vivo*,
631 Biofouling. 33 (2017) 676–689. https://doi.org/10.1080/08927014.2017.1356289.

632 [20] L. Zhang, J. Zhang, Y. Ling, C. Chen, A. Liang, Y. Peng, H. Chang, P. Su, D. Huang,
633 Sustained release of melatonin from poly (lactic-co-glycolic acid) (PLGA) microspheres
634 to induce osteogenesis of human mesenchymal stem cells in vitro, J. Pineal Res. 54 (2013)

635 24–32. https://doi.org/10.1111/j.1600-079X.2012.01016.x.

636 [21] J.R. Wiśniewski, A. Zougman, N. Nagaraj, M. Mann, Universal sample preparation
637 method for proteome analysis, Nat. Methods. 6 (2009) 359–362.
638 https://doi.org/10.1038/nmeth.1322.

639 [22] F. Romero-Gavilán, S. Barros-Silva, J. García-Cañadas, B. Palla, R. Izquierdo, M.
640 Gurruchaga, I. Goñi, J. Suay, Control of the degradation of silica sol-gel hybrid coatings
641 for metal implants prepared by the triple combination of alkoxysilanes, J. Non. Cryst.
642 Solids. 453 (2016) 66–73. https://doi.org/10.1016/j.jnoncrysol.2016.09.026.

643 [23] Y. Li, X. Zhao, Y. Zu, L. Wang, W. Wu, Y. Deng, C. Zu, Y. Liu, Melatonin-loaded silica
644 coated with hydroxypropyl methylcellulose phthalate for enhanced oral bioavailability:
645 Preparation, and in vitro-in vivo evaluation, Eur. J. Pharm. Biopharm. 112 (2017) 58–66.
646 https://doi.org/10.1016/j.ejpb.2016.11.003.

647 [24] M.J. Juan-Díaz, M. Martínez-Ibáñez, M. Hernández-Escolano, L. Cabedo, R. Izquierdo,
648 J. Suay, M. Gurruchaga, I. Goñi, Study of the degradation of hybrid sol-gel coatings in
649 aqueous medium, Prog. Org. Coatings. 77 (2014) 1799–1806.
650 https://doi.org/10.1016/j.porgcoat.2014.06.004.

651 [25] A.S. Vishnevskiy, D.S. Seregin, K.A. Vorotilov, A.S. Sigov, K.P. Mogilnikov, M.R.
652 Baklanov, Effect of water content on the structural properties of porous methyl-modified
653 silicate films, J. Sol-Gel Sci. Technol. 92 (2019) 273–281. https://doi.org/10.1007/s10971-
654 019-05028-w.

655 [26] M. Sabzichi, N. Samadi, J. Mohammadian, H. Hamishehkar, M. Akbarzadeh, O. Molavi,
656 Sustained release of melatonin: A novel approach in elevating efficacy of tamoxifen in
657 breast cancer treatment, Colloids Surfaces B Biointerfaces. 145 (2016) 64–71.
658 https://doi.org/10.1016/j.colsurfb.2016.04.042.

659 [27] S. Maria, P.A. Witt-Enderby, Melatonin effects on bone: Potential use for the prevention
660 and treatment for osteopenia, osteoporosis, and periodontal disease and for use in bone-
661 grafting procedures, J. Pineal Res. 56 (2014) 115–125. https://doi.org/10.1111/jpi.12116.

662 [28] A. Cutando, A. López-Valverde, S. Arias-Santiago, J. De Vicente, R.G. De Diego, Role
663 of melatonin in cancer treatment, Anticancer Res. 32 (2012) 2747–2754.

664 [29] L. Liu, Y. Zhu, Y. Xu, R.J. Reiter, Melatonin delays cell proliferation by inducing G 1 and
665 G 2 / M phase arrest in a human osteoblastic cell line hFOB 1 . 19, J. Pineal Res. (2011)
666 222–231. https://doi.org/10.1111/j.1600-079X.2010.00832.x.

667 [30] J.H. Son, Y.C. Cho, I.Y. Sung, I.R. Kim, B.S. Park, Y.D. Kim, Melatonin promotes

668 osteoblast differentiation and mineralization of MC3T3-E1 cells under hypoxic conditions
669 through activation of PKD/p38 pathways, J. Pineal Res. 57 (2014) 385–392.
670 https://doi.org/10.1111/jpi.12177.

671 [31] Z. Ping, X. Hu, L. Wang, J. Shi, Y. Tao, X. Wu, Z. Hou, X. Guo, W. Zhang, H. Yang, Y.
672 Xu, Z. Wang, D. Geng, Melatonin attenuates titanium particle-induced osteolysis via
673 activation of Wnt/β-catenin signaling pathway, Acta Biomater. 51 (2017) 513–525.
674 https://doi.org/10.1016/j.actbio.2017.01.034.

675 [32] N.H. Cho, S.Y. Seong, Apolipoproteins inhibit the innate immunity activated by necrotic
676 cells or bacterial endotoxin, Immunology. 128 (2009) 479–486.
677 https://doi.org/10.1111/j.1365-2567.2008.03002.x.

678 [33] J.F.P. Berbée, L.M. Havekes, P.C.N. Rensen, Apolipoproteins modulate the inflammatory
679 response to lipopolysaccharide, J. Endotoxin Res. 11 (2005) 97–103.
680 https://doi.org/10.1179/096805105X35215.

681 [34] P. Nesargikar, B. Spiller, R. Chavez, The complement system: History, pathways, cascade
682 and inhibitors, Eur. J. Microbiol. Immunol. 2 (2012) 103–111.
683 https://doi.org/10.1556/eujmi.2.2012.2.2.

684 [35] M.C. Carroll, The complement system in regulation of adaptive immunity, Nat. Immunol.
685 5 (2004) 981–986. https://doi.org/10.1038/ni1113.

686 [36] M.C. Carroll, The complement system in B cell regulation, in: Mol. Immunol., 2004: pp.
687 141–146. https://doi.org/10.1016/j.molimm.2004.03.017.

688 [37] T.E. Mollnes, M. Kirschfink, Strategies of therapeutic complement inhibition, Mol.
689 Immunol. 43 (2006) 107–121. https://doi.org/10.1016/j.molimm.2005.06.014.

690 [38] J.L. Mauriz, P.S. Collado, C. Veneroso, R.J. Reiter, J. González-Gallego, A review of the
691 molecular aspects of melatonin's anti-inflammatory actions: Recent insights and new
692 perspectives, J. Pineal Res. 54 (2013) 1–14. https://doi.org/10.1111/j.1600-
693 079X.2012.01014.x.

694 [39] J.R. Calvo, C. Gonzalez-Yanes, M.D. Maldonado, The role of melatonin in the cells of the
695 innate immunity: A review, J. Pineal Res. 55 (2013) 103–120.
696 https://doi.org/10.1111/jpi.12075.

697 [40] L.J. Druhan, A. Lance, S. Li, A.E. Price, J.T. Emerson, S.A. Baxter, J.M. Gerber, B.R.
698 Avalos, Leucine rich α-2 glycoprotein: A novel neutrophil granule protein and modulator
699 of myelopoiesis, PLoS One. 12 (2017) 1–13.
700 https://doi.org/10.1371/journal.pone.0170261.

[41] S. Park, W. Jang, E. Yi, J. Jang, Y. Jung, J. Jeong, Y. Kim, Melatonin suppresses tumor angiogenesis by inhibiting HIF-1α stabilization under hypoxia, J. Pineal Res. 48 (2010) 178–184. https://doi.org/10.1111/j.1600-079X.2009.00742.x.

[42] K. Kim, J. Choi, I. Kang, K. Kim, C. Jeong, J. Jeong, Melatonin suppresses tumor progression by reducing angiogenesis stimulated by HIF-1 in a mouse tumor model, J. Pineal Res. 54 (2013) 264–270. https://doi.org/10.1111/j.1600-079X.2012.01030.x.

[43] Y. Wu, Contact pathway of coagulation and inflammation, Thromb. J. 13 (2015) 17. https://doi.org/10.1186/s12959-015-0048-y.

[44] J.C. Chapin, K.A. Hajjar, Fibrinolysis and the control of blood coagulation, (2014). https://doi.org/10.1016/j.blre.2014.09.003.

[45] D. V. Sakharov, J.F. Nagelkerkel, D.C. Rijken, Rearrangements of the fibrin network and spatial distribution of fibrinolytic components during plasma clot lysis: Study with confocal microscopy, J. Biol. Chem. 271 (1996) 2133–2138. https://doi.org/10.1074/jbc.271.4.2133.